

DIMENSIONING OF COOLING FINN FOR HIGH-AMPERAGE REDUCTION CELLS

I. Eick and D. Vogelsang

VAW Aluminium-Technologie GmbH

Georg-von-Boeselager Str. 25

53117 Bonn, Germany

Abstract

The heat generated in the bath region of high-amperage reduction cells has to be dissipated in a controlled manner to establish a stable side ledge which protects the potlining sufficiently. This can be achieved by designing the potlining of the cells using thermo-electric simulations which also take into account the cooling effect of the shell cradles. In cases of spatial restrictions, due to short distances inside the pot, strong metal flow against the ledge or insufficient ventilation between the pot shells, additional cooling fins welded to the pot shell can be used to avoid “hot spots” and vanishing side ledge thickness.

The position and dimensions of such cooling fins can be designed using Computational Fluid Dynamics (CFD) simulations of the heat transfer conditions, assuming turbulent natural convection of the ambient air. The local heat transfer coefficients determined in this way can be implemented in thermo-electric heat balance models, thus offering the possibility to optimize the dimensions of the cooling fins and to analyze the impact of different ventilation conditions. Examples of computational results for different fin configurations are given. The calculated temperature fields and heat fluxes are compared to corresponding plant measurements.

Introduction

Driven by the economic attractiveness of exploiting the installed capacity to the utmost, aluminium smelters around the world are increasing amperage beyond the technological design limit. This general trend, often called “capacity creep”, runs the risk of being accompanied by a deterioration in the magneto-hydrodynamic performance of the pots

and a disturbance of the energy balance with the disadvantage of loosing side ledge and premature pot failures. Increasing the current load above its design limit of the cell technology installed typically results in an enhanced tendency towards magneto-hydrodynamic instabilities (“metal pad roll”). This normally causes an increase in the equilibrium anode-cathode distance and a corresponding increase in the mean heating power.

The electromagnetic forces driving the metal and bath-flow field also increase with the higher current load. Hence, the heat transferred from the liquid metal and bath to the side ledge is intensified and may result in a weakening of the cell’s side ledge. From this, it is obvious that, at the boosted amperage, effects associated with the magneto-hydrodynamics of the cell result in an increase in the thermal load on the cell’s sides. This direct rise in the thermal load is caused by the increase in the heating power of the reduction cell due to the higher amperage. About 50 % of the surplus of the energy input – compared with the design value for the cell technology installed – must be dissipated as heat losses mainly along the long sides of the cell.

There are two ways of coping with the excess of heating power to be dissipated: through the installation of modified cathodes and/or modification to the pot shell to sustain an increased heat transfer to the ambience. The installation of modified cathodes with a change over from semigraphitic to fully graphitized blocks is often done in conjunction with the anticipated increase in current load. A certain drawback of this migration path is the long-lasting coexistence of different cathodes in the potroom population. However, due to the better thermal conductivity of fully graphitized blocks, the extra amount of heating power can be dissipated to a certain degree due to the higher pot-shell temperatures.

To avoid too high shell temperatures that could result in a

weakening of the shell stiffness, additional cooling fins are often welded in this case to critical sections of the shell structure. In the following, some general remarks about governing heat transfer mechanism from the cell interior to the ambience are made. Design criteria for cooling fins are given and the impact on the heat transfer coefficient is clarified and compared to plant measurements. The convective heat transfer caused by the additional cooling fins was evaluated using the CFD code FIDAP. The resulting heat transfer coefficients were subsequently introduced into the fully 3-dimensional thermo-electrical Finite-Element model of reduction cells. This step-by-step approach results in a more realistic description of the boundary conditions and their impact on the calculated side ledge contour, temperature field and heat balance for a given load case.

Conductive Heat Transfer

A simple 1-dimensional estimate for the description of the heat transfer from the interior of the cell to the ambience can be used to determine the maximum heat loss of the shell at the height of the metal/bath interface and the maximum shell temperature T_w , cf. Figure 1.

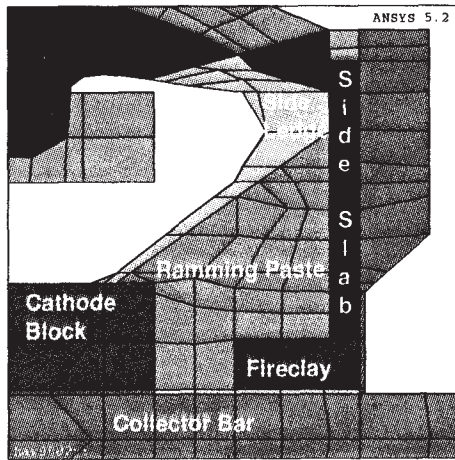


Figure 1: Geometry of the cell model

The heat transfer resistances due to convection at the side ledge R_{in} and shell R_{out} are added up together with the resistances of the conducting materials to give the total heat transfer resistance R_{tot} :

$$R_{tot} = R_{in} + R_{ledge} + R_{ramm} + R_{slab} + R_{shell} + R_{out} \quad (1)$$

Note that the convective heat transfer resistance is defined as $R_i = 1/\alpha_i$ with the heat transfer coefficient α_i [W/m^2K]. The conductive resistances $R_i = d_i/\lambda_i$ are calculated using the thickness d_i of a material and its conductivity λ_i for the side ledge, ramming paste, side slab and shell plate. For the heat transfer coefficients at the side ledge, a value of $800 W/m^2K$ is reasonable [3] although this value depends on the flow pattern of the liquid bath and metal. For the heat transfer coefficient of the steel plate, a value of 18-20 W/m^2K can be taken from plant measurements. The following table gives this 1-dimensional estimate for a 165 kA reduction cell:

Region	d [m]	λ [W/mK]	α [W/m^2K]	R [m^2K/W]
Bath → Ledge	-		800	0.0013
Ledge	0.088	1.2		0.0733
Ramming	0.153	5.2		0.0294
Side slab	0.060	24.		0.0025
Steel shell	0.019	44.		0.0004
Shell → Air	-		18.6	0.0538
Bath → Air	0.320			0.1607

From the example shown, the maximum total heat flux can be estimated, assuming a bath/metal temperature of $T_{in} = 940^\circ C$ and a reference temperature $T_0 = 15^\circ C$ for the ambience, to be $q_{tot} = 5,756 W/m^2$. From this value, the maximum shell temperature can be calculated, i.e. $T_w = T_{bath} - q_{tot} * R_{inside} = 324^\circ C$. Both figures are an upper estimate because the general heat flux direction perpendicular to the shell wall neglects heat fluxes in the vertical direction, especially within the side slab. For the heat transfer resistance to the ambience at the shell wall (R_{out}), the combined heat transfer mechanism comprising conduction, convection and radiation, has to be taken into account. From elemental heat transfer theory for this network of parallel heat transfer resistances we get:

$$R_{out} = \frac{1}{\frac{1}{R_{cond}} + \alpha_{conv} + \alpha_{rad}} \quad (2)$$

where the thermal conductive heat flux of the shell

$$q_{cond} = 1/R_{cond} * (T_w - T_0) \quad (3)$$

is very small and can be treated as part of the convective heat flux. In the following sections, estimations for the heat fluxes due to convection and radiation will be given and subsequently refined by means of a 3-dimensional Computational Fluid Dynamics (CFD) approach.

Convective Heat Transfer

Natural convection caused by the buoyancy flow field of hot air at the steel shell and forced convection, e.g. due to external wind forces, have to be taken into account to determine the total convective heat transfer at the shell's side. Both can be treated using proven expressions for the Nusselt number (Nu), thermal conductivity of the hot air (λ_{air}) and the height of the flow length at the shell (h):

$$q_{conv} = \alpha_{conv} * (T_w - T_0) \quad (4)$$

$$\text{with } \alpha_{conv} = Nu \lambda_{air}/h \quad (5)$$

For a high shell temperature and a long acceleration path along the shell, the convection flow with the local velocity $u_{conv} \approx \sqrt{g \beta_{air} (T_w - T_0) h}$ becomes turbulent. The corresponding Reynolds number is easily described by $Re = \sqrt{Ra}$, see [4].

The Nusselt number describing the turbulent natural convective heat transfer (Nu_{nat}) is best expressed as a function of the Rayleigh and Prandtl number according to the following equation, see [5]:

$$Nu_{nat} = \left[0.825 + 0.387 (Ra * f(Pr))^{1/6} \right]^2 \quad (6)$$

with $f(Pr) = \frac{1}{(1 + (\frac{0.492}{Pr})^{9/16})^{16/9}} = 0.348$ for $Pr \approx 0.7$.

Calculated Nusselt numbers for natural convection are plotted in Figure 2 against the temperature of the shell's wall. For the typical temperature range of 300-350°C, the Nusselt number can be estimated to be about $Nu_{nat} = 500$.

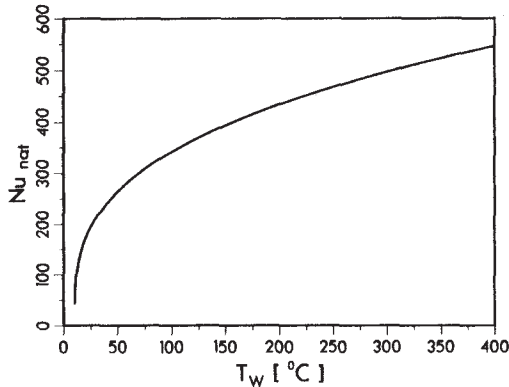


Figure 2: Natural convection versus shell temperature.

A tremendous increase in the total heat flux can be achieved by applying an external air flow to the shell's side, e.g. wind flow or, in the extreme case, the application of air lances. In this case the Nusselt number representing the impact of the external air flow (Nu_{ext}) is best described using the following relations for the laminar ($Re < 10,000$) and turbulent flow condition ($Re > 400,000$) along a vertical plate:

$$Nu_{lam} = 0.664 \sqrt{Re} \sqrt[3]{Pr} \tag{7}$$

$$Nu_{turb} = \frac{0.037 Re^{0.8} Pr}{1 + 2.443 Re^{-0.1} (Pr^{2/3} - 1)} \tag{8}$$

$$Nu_{ext} = \sqrt{Nu_{lam}^2 + Nu_{turb}^2} \tag{9}$$

Together with the Nusselt contribution resulting from natural convection, the total Nusselt number for the vertical plate case is finally calculated to be:

$$Nu_{tot} = \sqrt[3]{Nu_{nat}^3 + Nu_{ext}^3} \tag{10}$$

In Figure 3, the total Nusselt number is plotted against the air velocity u_{conv} [m/s]. For typical air velocities near reduction shell plates of 2-4 m/s, the total heat transfer is larger than the just calculated for natural convection by a factor of two.

Heat Transfer by Radiation

The third contribution to the total heat flux can be attributed to radiation. Denoting shell wall and ambience temperature as absolute temperatures T_{WK} and T_{0K} , respectively, the Boltzmann law yields the following expression for the corresponding heat flux:

$$q_{rad} = \frac{\epsilon \varphi \sigma}{A} (T_{WK}^4 - T_{0K}^4) \tag{11}$$

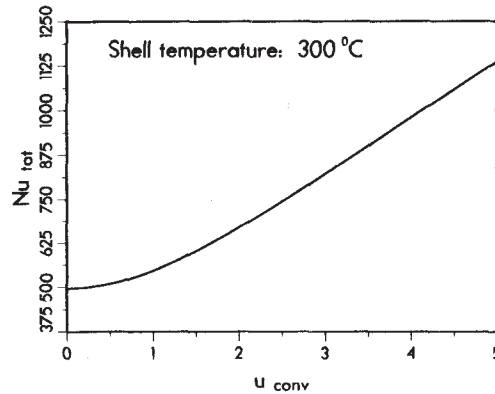


Figure 3: Forced convection versus air velocity.

The proportionality is defined by the Boltzmann constant σ , the emissivity of the shell, $\epsilon = 0.95$, the viewfactor φ between the hot shell to the surroundings and the shell size A . A heat transfer coefficient for the radiation can be defined by dividing equation (11) by the temperature difference from shell to the air, $\Delta T_W = (T_{WK} - T_{0K})$:

$$\alpha_{rad} = \frac{\epsilon \varphi \sigma (T_{WK}^4 - T_{0K}^4)}{A (T_{WK} - T_{0K})} \tag{12}$$

All three heat fluxes add up to a total heat transfer coefficient which will be studied in the following section:

$$\alpha_{tot} = \frac{\lambda_{air}}{d_{air}} + Nu_{tot} \frac{\lambda_{air}}{h} + \frac{\epsilon \varphi \sigma (T_{WK}^4 - T_{0K}^4)}{A (T_{WK} - T_{0K})} \tag{13}$$

The individual contribution of the three governing heat transfer mechanisms – conduction, convection and radiation – is given in Figure 4 as a function of the shell wall temperature on a logarithmic scale.

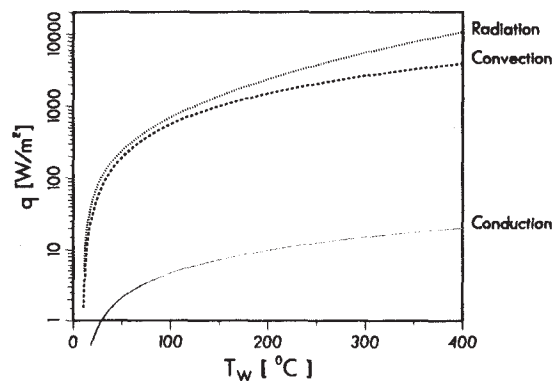


Figure 4: Heat Flux due to conduction, convection and radiation.

The smallest part of some W/m^2 is caused by conduction, while up to about 100°C convection as well as radiation contribute the same amount with heat fluxes of some 1,000 W/m^2 . Radiation becomes more and more prominent for

shell temperatures above 100 °C and, for shells with temperatures as high as 400°C, radiation causes about 65 % of the total heat losses.

Convective/Radiative Shell Model

The expressions for the total heat loss as given in the previous section giving a rough estimate of the maximum shell temperature and heat losses with respect to some few additional information like bath and ambient temperature and air velocity. However, the underlying elemental heat transfer theory implies heat transfer along a vertical wall with constant temperature and without cradles. To gain additional information regarding the influence of realistic shell temperature fields and geometries of shell wall and cradles, a fully 3-dimensional CFD model was developed based on the CFD code FIDAP. The model comprises coupled turbulent convection as well as radiation. The actual example is taken from a 165 kA reduction cell with experimental shells equipped with four cooling fins between two adjacent cradles. Plant measurements of shell temperature and heat flux for these experimental pots and standard pots with plain pot shells indicate a feasible effect on the maximum shell temperature and heat flux [9]. The geometry of the solution domain comprising half a shell section between two adjacent cradles and cooling fins is given in Figure 5.

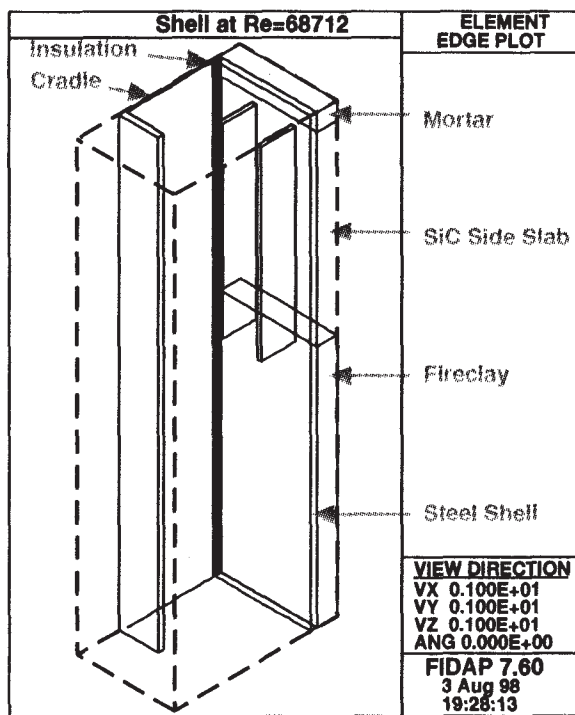


Figure 5: Geometry of the convection model

Note, that in the actual example the steel cradles are not fully welded to the shell wall. This insulating effect in the contact zone was modelled by a thin insulating board with a thermal conductivity of 1.7 W/mK. The thermal boundary condition of the interior side of the cell was taken as a temperature field for the side slab and lining material. These values were calculated using the fully 3-dimensional thermo-electrical reduction cell model described previously [1, 2]. The results

of this model agree well with plant measurements [8, 9]. The implementation of the convective/radiative shell model using the CFD code FIDAP features the following approximations:

- The simulation was performed assuming natural convection, only. Hence the predicted results can be regarded as a worst case simulation of the cooling conditions. For the buoyancy driven convection flow, the Boussinesq approximation of an incompressible fluid was used [7].
- As discussed above, the natural convection at a 300 °C hot shell is a weak turbulent flow with a Reynolds number of $Re \approx 68,000$. Therefore a K.E.-model with a high dissipation rate of 5% was used. Tests with the Mixing-Length-model resulted in the same order of thermal and momentum boundary layer thickness.
- The radiation was included as a black body radiation term. Alternative solutions based on grey radiation with a detailed viewfactor calculation yielded similar results assuming a high emissivity steel shell with $\epsilon = 0.95$. For standard calculations, however, this approach turned out to be too much storage intensive.

Temperatures in the inflow area at the bottom of the flow region and at the side opposite the shell, the “infinite area”, were set to the reference temperature $T_0 = 15^\circ\text{C}$.

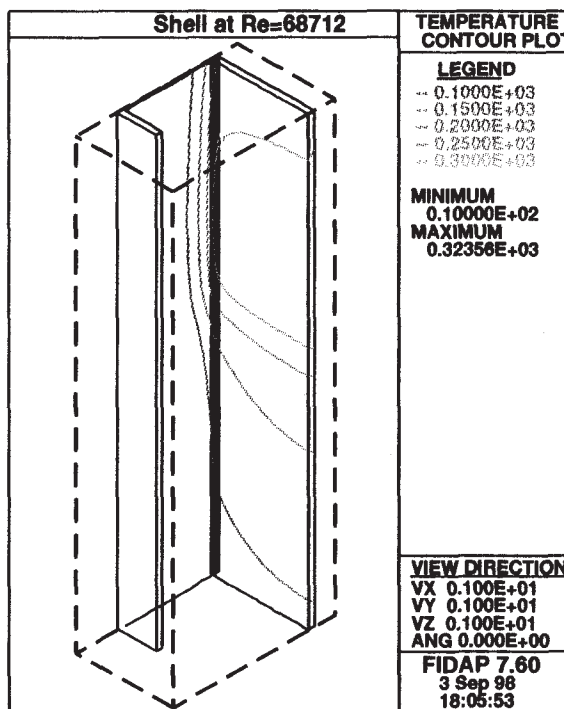


Figure 6: Temperatures of a plain shell

The left and right sides of the flow region are symmetry planes and no crossover of the air flow was allowed. The top face, i.e. the outflow area, was subject to an environmental pressure condition. Normally the “infinite area” will

be restricted by the busbar system. Therefore only a vertical flow was allowed. Heat exchange with the busbars was not considered.

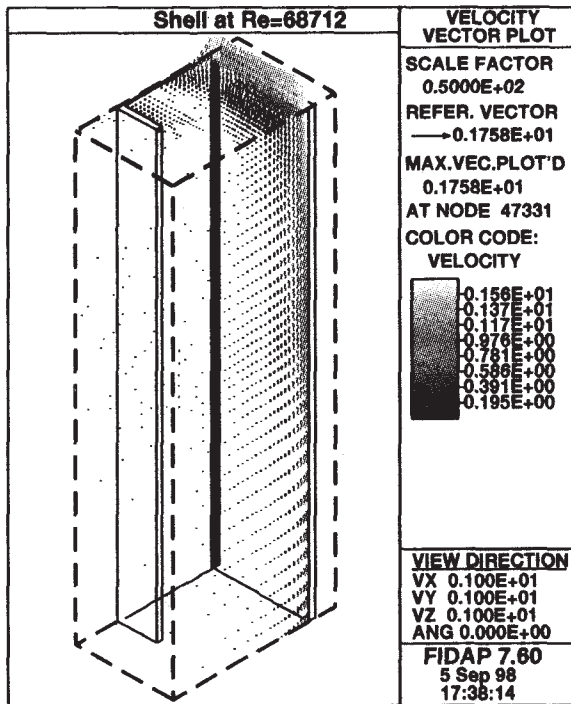


Figure 7: Convective flow field at a plain shell

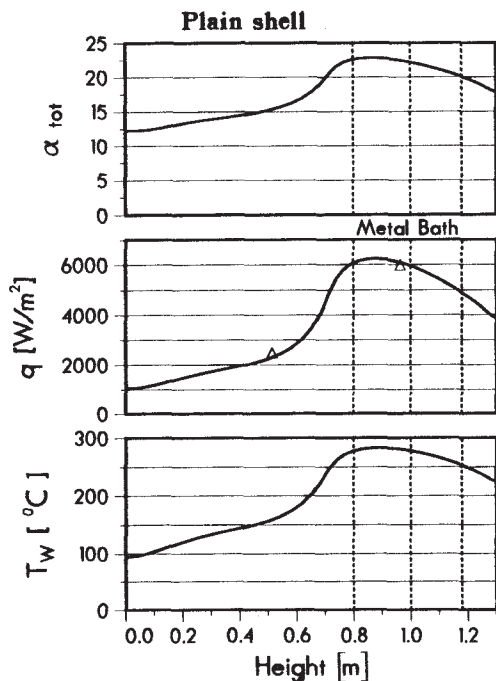


Figure 8: Shell temperature, total heat flux and total heat transfer coefficient at a plain shell

Figure 6 depicts the temperature distribution of the plain shell before installing the cooling fins. In the center between

the cradles and at the height of bath and metal, there is a hot area of about $T_{W_{max}} = 323^{\circ}C$. The corresponding velocity vector field of the ambient air is shown in Figure 7.

The plot indicates the increasing air velocities with increasing shell height. The maximum velocity at the upper border of the shell was calculated to be 1.8 m/s . Along the right hand side symmetry plane of the model, the shell temperature, total heat flux and total heat transfer coefficient were plotted versus the shell height, c.f. Figure 8.

The maximum convective heat flux in the hot area is expected to be about $6,000 \text{ W/m}^2$. Two measured heat fluxes are given in the plot as little triangles. The agreement with the calculated fluxes is reasonable. The total heat transfer coefficient as defined by equation (13) starts at the shell bottom of about 12 W/m^2K and increases in parallel with temperature and total heat flux to a maximum of 22 W/m^2K .

The impact of four cooling fins measuring $12 \times 100 \times 515 \text{ mm}$, cf. Figure 5, was simulated applying similar boundary conditions as those for the plain shell case. In particular, the thermal boundary condition in the interior of the cell was kept. Preliminary simulations with the thermo-electrical model indicate that the temperature field along the interior side of the side slab is affected only to a minor degree by the heat transfer coefficient at the shell boundary.

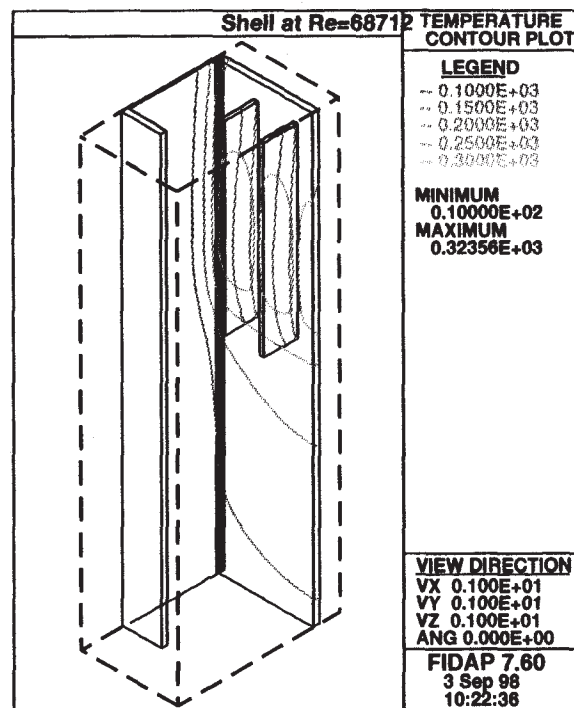


Figure 9: Temperature at the shell with cooling fins

Figure 9 depicts the temperature distribution of the shell with cooling fins and should be compared with Figure 6. The hot area in the center between the cradles is now divided by the fins, as can be seen from the appearance of the $250^{\circ}C$ contour line. In the chimney-like area between cradle and the left cooling fin, the convective flow field in Figure 10 is significantly broadened compared with the plain shell case. The maximum velocity is slightly reduced by about 0.1 m/s .

More detailed information is given in Figure 11 for the shell temperature, total heat flux and total heat transfer coefficient.

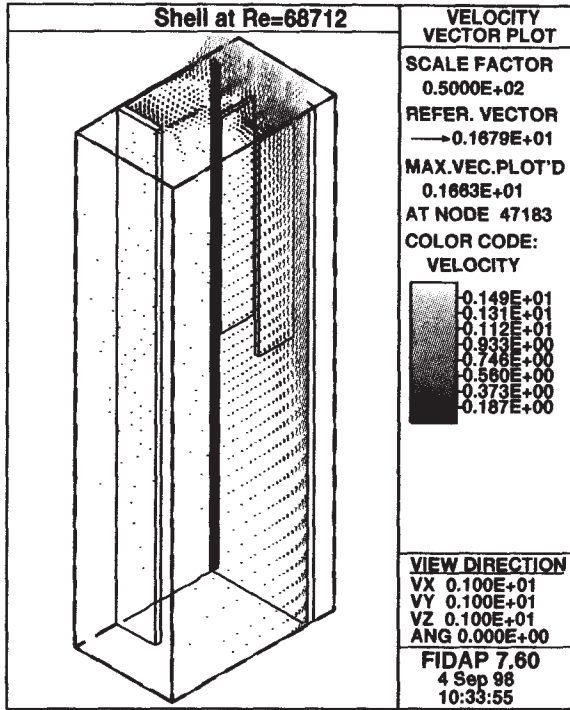


Figure 10: Convective flow field at the shell with cooling fins

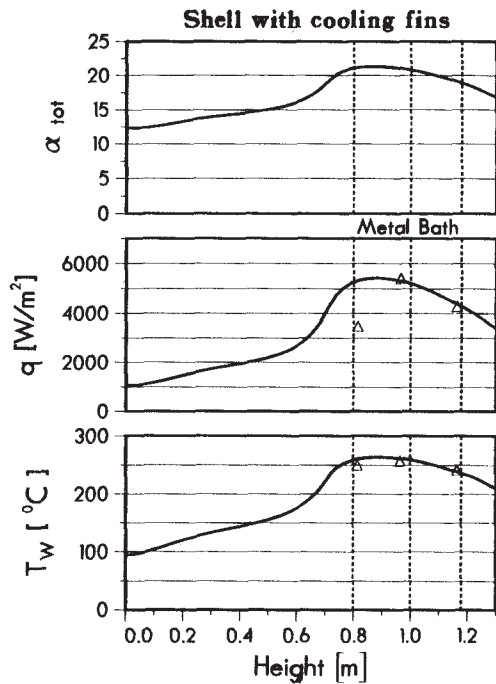


Figure 11: Shell temperature, total heat flux and total heat transfer coefficient at shell with cooling fins

The measured values for the shell temperature and heat flux at three different heights agree reasonably with the predicted natural convection case. Compared to the plain shell case in Figure 8, the maximum shell temperature in the hot area at the height of the metal pad is reduced by about 20 °C and the corresponding heat flux is lowered by about 500 W/m².

One can conclude that the main effect of the cooling fins was not to increase the heat flux of the shell but to distribute the temperature loads and protect the shell from overheating and subsequent thermal deformations. In cases of critical cell states and strong metal pad flow directed towards the cell sides, the fins will enlarge the effective radiation surface and ensure a stable convection flow at its outer region.

Designing Cooling Fins

To configure the cooling fins in an appropriate way, the flow pattern of the convective air flow has to be considered and the thermal and momentum layer has to be estimated. For the shell with the cooling fins, both boundary layers are plotted in Figure 12 against the distance to the shell for 3 different heights at the shell.

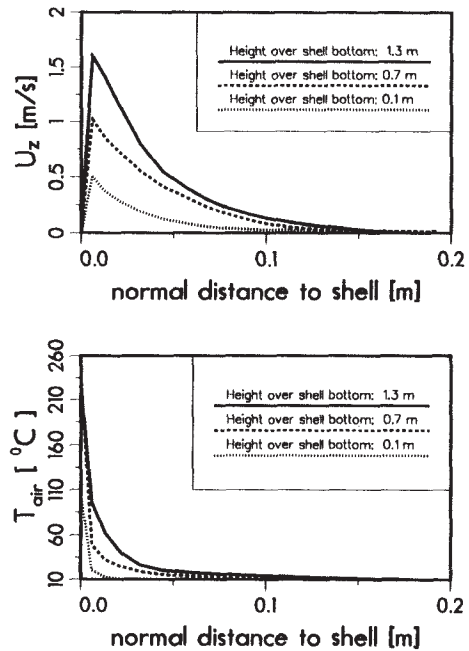


Figure 12: Temperature distribution and velocity profile at the shell

The thickness of both boundary layers depends on the convection velocity, hence on the Reynolds number, that is increasing along the convection path. The ratio is proportional to the Prandtl number $Pr \approx 0.7$.

If two fins are very close to each other, the boundary layer of both sides merge and a hot air corridor can occur between the fins. In this case the temperature difference driving the convection becomes too small and the total heat flux stagnates. The radiative shell is then faced with a hot air wall which further reduces the radiating heat flux. In extreme cases, the situation becomes worse compared with the plain shell case. Therefore, the distance between the fins should be larger than the momentum boundary layer. The depth and thickness of the fins should be optimized by the heat flux function of a fin at a constant air temperature [10],

$$q_{fin} = \alpha_{fin} \Delta T_W \frac{\tanh(Md)}{Md}; \quad M = \sqrt{\frac{2\alpha_{fin}}{\lambda_{fin} b}} \quad (14)$$

At least with a depth of $d = 20$ cm, which will be large enough to reach outside the thermal boundary layer, and a thickness $b = 1.5$ cm based on a 20 cm wide shell strip the heat flux could be increased by 76% compared to the plane shell.

Conclusion

The general trend of exploiting the installed smelter capacity by boosting the amperage beyond the technological design limit results in a surplus of heating power that has to be dissipated along the shell sides. From a 1-dimensional model, the governing contribution made by conduction, convection as well as radiation can be estimated. This allows a rough prediction of the maximum shell temperature and heat flux. The total heat flux of the thermal shell losses is mainly governed by the combined convective/radiative effects. More detailed information can be gained by a fully 3-dimensional convective/radiative model of the steel shell. Such a model is developed and allows the prediction of the impact of additional cooling fins welded to the shell plate on the total heat losses. For an actual example, reasonable agreement between the measured and calculated shell temperature and heat flux was found, assuming the case of natural convection. Choosing the dimension as well as the location of the cooling fins welded to the shell plate, the size of the thermal and momentum boundary layer has to be taken into account to prevent in extreme cases a worsening of the situation compared to the plain shell case.

Acknowledgment

Special thanks are due to J. Prepenit and E. Sturm of Hamburger Aluminium Werke for fruitful discussions and the acquisition of plant measurements.

Notation

β_{air}	[1/K]	Thermal expansion coefficient of air
η_{air}	[kg/ms]	Dynamic viscosity of air
λ_{air}	[W/mK]	Thermal conductivity of air
ρ_{air}	[kg/m ³]	Density of air
α	[W/m ² K]	Heat transfer coefficient
Q	[W]	Heat
q	[W/m ²]	Heat flux

i	Counter index
K	Index for temperatures in Kelvin
w	Index for entities at the shell wall
x, y, z	Index of x,y,z direction
0	Index for reference values

$g = 9.81$	[m/s ²]	Gravitation acceleration
$\sigma = 5.67E - 8$	[W/m ² K ⁴]	Boltzmann constant
$T_K = -273.17$	[°C]	Kelvin temperature
$\mu = \frac{\eta}{\rho}$	[m ² /s]	Kinematic viscosity
$Nu = \frac{\alpha d}{\lambda}$	[]	Nusselt number
$Pr = \frac{c_p \eta}{\lambda}$	[]	Prandtl number
$Re = 1/\mu U^* L^*$	[]	Reynold number
$Gr = \frac{g \beta (T_w - T_0) h^3}{\mu^2}$	[]	Grashof number
$Ra = Gr * Pr$	[]	Rayleigh number

References

1. D. Vogelsang, *Application of Process Modelling to Improve Aluminium Production*, 6th. Australasian Aluminium Smelter Techn. Workshop, 22-27 November 1998.
2. D. Vogelsang, I. Eick, Ch. Droste, M. Segatz *From 110 to 175 kA: Retrofit of VAW Rheinwerk - Part I: Modernization Concept*, Light Metals 1997, pp. 233-238.
3. M.P. Taylor and B.J. Welch, *Melt/freeze Heat Transfer Coefficients: Experimental Determination and Industrial Application*, Light Metals 1985, pp. 781-789.
4. W.M. Kays, M.E. Crawford, *Convective Heat and Mass Transfer*, McGraw-Hill Inc., New York, 1993.
5. B. Gebhart, *Correlating equations for laminar and turbulent free convection from a vertical plate*, J. Fluids Engng, Vol 101, pp. 5-28, 1979.
6. Verein Deutscher Ingenieure, *VDI-Wärmeatlas*, VDI-Verlag, Düsseldorf, 1994.
7. FIDAP7.0 *Theoretical Manual*, Fluid Dynamics International Inc., Evanston, Revision 7.0 - April 1993.
8. G. Loßmann, *Utilization of various measurements in reduction cells for operational improvement*, Light Metals 1992, pp. 441-447.
9. J. Prepenit, E. Sturm, *Private communications*, Hamburger Aluminium Werke, Germany, 1998.
10. Hell, Friedrich, *Grundlagen der Wärmeübertragung*, VDI - Verlag, Düsseldorf, 1982.